This is a repository copy of *Early stages of pitting corrosion of UNS K03014 carbon steel in sour corrosion environments: The influence of CO2, H2S and temperature*.

White Rose Research Online URL for this paper:
http://eprints.whiterose.ac.uk/92551/

Version: Accepted Version

## Proceedings Paper:

**Early stages of pitting corrosion of UNS K03014 carbon steel in sour corrosion environments:**

**The influence of $CO_2$, $H_2S$ and temperature**

Frederick Pessu, Richard Barker and Anne Neville
Institute of Functional Surfaces (iFS)
School of Mechanical Engineering,
University of Leeds.
Leeds,
LS2 9JT, UK

The challenges in managing localized corrosion failures in oilfields are of serious concern. In environments containing both $CO_2$ and $H_2S$ gas, pitting corrosion of carbon steel is considered to be a common occurrence and particularly complex. The actual mechanisms and sequence of electrochemical activities for pitting corrosion in these environments is still not fully understood. The film formation characteristics and morphology in $CO_2$ and $H_2S$-containing systems is also known to influence the pitting corrosion behavior of carbon steel. However, questions still remain as to how the combined presence of $CO_2$ and $H_2S$ gas both influence the corrosion mechanisms, as well as pit initiation and propagation. This paper presents part of an ongoing parametric study to investigate pitting corrosion behavior of carbon steel in $CO_2/H_2S$-containing environments. The work presented explores the impact of changes in two key process parameters (namely; temperature, absence/presence of 10% $H_2S$ and absence/presence of $CO_2$ in the gas phase) on the early process of pitting corrosionon carbon steel in NaCl brines. A pit initiation study is conducted up to 7 hours based on changes in temperature and presence/absence of $H_2S$ gas. Corrosion film properties and morphology are studied through a combination of electrochemical and surface analysis techniques which include scanning electron microscopy (SEM) and X-ray diffraction (XRD). The extent of corrosion damage of the carbon steel is evaluated through the implementation of surface interferometry to study discrete pit geometry; namely, the size and depth. The results show that the depths of pits initiated after 7 hours were higher in $H_2S$-containing environments (10% $H_2S$ in the gas phase), while general corrosion rates dominate the degradation mechanism when $CO_2$ gas is solely present.

KEY WORDS: Carbon dioxide corrosion, hydrogen sulfide corrosion, Iron sulfide, uniform corrosion, pitting, localized corrosion.

## INTRODUCTION

In the oil and gas industry, corrosion related failures have been reported to constitute over 25% of total safety incidents[1,2]. The problem of corrosion in oilfield environments is mainly associated with the presence of dissolved acidic gases in reservoir brines, namely $CO_2$-containing (sweet) and $H_2S$-containing (sour) systems[2,3]. Pitting corrosion remains one of the main modes of corrosion related failures encountered during oilfield production, constituting 12% of all oilfield corrosion incidences[1] and generating a significant impact on the economics of production[1,2].

This localised mode of corrosion is of particular concern because of its unpredictable nature and the difficulty associated with inhibiting pit propagation once it has initiated.Such incidences of pitting corrosion failures are commonly encountered in oil and gas pipelines exposed to $CO_2$-$H_2S$ saturated brines[4-6]. The tendency for pits to initiate and propagate in an un-buffered corrosion environment can be influenced by environmental and physical factors [7].

The corrosion mechanisms associated with both $CO_2$ and $H_2S$-containing environments can be generalised using the following reactions [2];

In $CO_2$ systems:  $Fe + H_2CO_3 \rightarrow FeCO_3 + H_{2\,(g)}$ (film formation)  (1)

In $H_2S$ systems:  $HS^- + e^- \rightarrow H + S^{2-}$  (2a)

$xFe + yH_2S_{(aq)} \rightarrow Fe_xS_y + yH_2$  (2b)
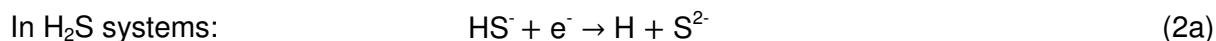
The generic equations of 2b with arbitrary stoichiometric annotations are often used to reflect the intrinsic complexities associated with sour corrosion and formation of an Iron sulfide film[8].

Pitting corrosion attack in $CO_2$-$H_2S$ saturated environments is such that it is strongly influenced by the independent reaction kinetics of $CO_2$ and $H_2S$ corrosion as well as the rate of $FeCO_3$ and $Fe_xS_y$ precipitation. It has been suggested that $H_2S$ corrosion is primarily dominated by two electrochemical processes; "solid state" corrosion reaction and aqueous phase corrosion reactions[9-11]. The former is a direct heterogeneous chemical reaction between $H_2S$ and Fe at the steel surface leading to the formation of iron sulfide films; mainly *mackinawite*[12], while in the later reaction, $H_2S$ acts as a corrosive specie like every other dissolved acidic gases that influences the cathodic process[9]. However, a clear understanding of the level of influence and/or interaction of the combining gases on pitting corrosion in these systems has remained elusive. It is also important to understand how other parameters such as temperature (in the case of this work) could be influencing the envisaged interaction and/or influence of the combining $H_2S$-$CO_2$ gases. It has also been reported that the initial layer of *mackinawite* formed in $H_2S$-containing environments is usually very thin and susceptible to failure which may lead to localized corrosion/pitting. This is somewhat dependent on the level of saturation with respect to $Fe^{2+}$ and $HS^-$ ions, as well as other environmental parameters [8,9,13,14]. The FeS films formed in sour corrosion systems have also been reported to be electronically conductive, with potential to generate local galvanic cells around unprotected  areas of steel surface, creating electrode potential gradients to drive the pitting process[15].

Several studies on the mechanism of corrosion in $H_2S$-containing environments have presented contrasting viewpoints on the effect of $H_2S$ gas on the corrosion of carbon steel in mixed $CO_2$-$H_2S$ containing environments. Videm and Kvarekvål[16] reported an increase of uniform corrosion rate of carbon steel in mixed $CO_2$-$H_2S$ containing environments with small amounts of $H_2S$ gas. On the other hand, Zheng et al.[17] and Ma et al.[14] reported a decrease in general corrosion rate of carbon steel in mixed $CO_2$-$H_2S$ and $H_2S$-containing environments, respectively with small amounts of $H_2S$ gas. Zheng et al.[17] attributed this effect to the inhibition of the reduction of $H_2CO_3$, but with no consideration to the formation of iron sulfide film, while Ma et al.[14] on the other hand suggested that such observation was due to the influence of the formation of iron sulfide film in a $H_2S$-containing acidic environment. Other authors have also reported an increase in general corrosion rate of carbon steel with an increase in $H_2S$ concentration and/or partial pressure up to 36 kPa in both mixed $CO_2$-$H_2S$ and pure $H_2S$-containing environments at 30ºC[17-19]. Such conflicting observations suggest a lack of clarity on this subject, especially since there is only limited literature on the interaction between $CO_2$ and $H_2S$. The effect of other environmental parameters on the corrosion damage morphology of carbon steel in mixed $CO_2$-

$H_2S$ containing environment still remains unclear. It must also be emphasized that steel may experience pitting corrosion as observed by Brown and Nesic[20]. Little research has been conducted to help understand the role of the combining gases ($CO_2$ and $H_2S$) and corrosion product formation, composition and morphology ($FeCO_3$ and $FeS$) on the localized corrosion of carbon steel in mixed $CO_2$-$H_2S$ environment.

It is therefore important as part of this research to explore parametric (temperature and $H_2S/CO_2$ presence/absence) based experimental routes to elucidate some aspects of pitting corrosion of carbon steel materials in $H_2S$-$CO_2$ environments. The results will be aimed at answering questions related to pitting corrosion initiation in sour conditions. This approach will help to isolate the role of $CO_2$ and $H_2S$ gas presence on the general and localized corrosion damage of carbon steel in $CO_2/H_2S$-containing environments, as well as the influence of temperature during the early stages of corrosion. Aspects such as the possible role $Fe_xS_y$ corrosion films will be explored.

## EXPERIMENTAL PROCEDURE

The purpose of this work was to assess the corrosion behavior of UNS K03014 steel exposed to three different gas systems; a pure $CO_2$ gas system, a $CO_2$-$H_2S$ gas system and a $N_2$-$H_2S$ gas system, all dissolved in a 3.5 wt.% NaCl solution at different temperatures (30°C, 50°C and 80°C). The emphasis of this study will include corrosion product formation, uniform and pitting corrosion quantification for short term experiments up to 7 hours to determine the role the film formation and environment plays on the general and localized corrosion behavior of the steel substrate. Temperatures and partial pressures of the gases within the system are provided in the matrix in Table 1.

**Table 1: Temperature of experiments and associated partial pressures of gases at atmospheric pressure in the tested brine solution**

| Temperature (ºC) | Partial Pressure, p (bar) |
|---|---|
| 30 | 0.97 |
| 50 | 0.89 |
| 80 | 0.55 |

Materials: UNS K03014 carbon steel samples were used as the working electrode in a three electrode electrochemical cell. The composition of UNS K03014 steel is provided in Table 2. The carbon steel was sectioned into 10 mm x 10 mm x 5 mm samples. Wires were soldered to the back of each test specimen and then embedded in a non-conducting resin. Prior to the start of each experiment, test samples were wet ground up to 1200 silicon grit paper, degreased with acetone, rinsed with distilled water and dried with compressed air before immersion into the test brine. A surface area of 1 $cm^2$ was exposed to the electrolyte for each sample.

**Table 2: UNS K03014 Carbon steel composition (wt.%)**

| C | Si | P | S | Mo | Mn | Ni | Nb | V | Fe |
|---|---|---|---|---|---|---|---|---|---|
| 0.15 | 0.22 | 0.025 | 0.002 | 0.17 | 1.422 | 0.09 | 0.054 | 0.057 | 97.81 |

Experimental setup: Sweet and sour corrosion experiment were conducted using separate bubble cell systems, but with the same sample surface area to brine volume ratio of 5 $cm^2$ per 1 liter of test solution maintained at the start of all tests. $CO_2$ corrosion experiments were conducted in two vessels which were each filled with 2 liters of brine. The vessels were sealed in every test with 10 samples immersed per vessel and $CO_2$ was bubbled into the test solution continuously to ensure complete saturation of the solution. Sour corrosion experiments were also conducted in two vessels which were each filled with 1 litre of brine, but only 5 samples

were present in this case. Pre-mixed 10 mol.% $H_2S$ – 90 mol.% $CO_2$ gas and 10 mol.% $H_2S$ – 90 mol.% $N_2$ gas were bubbled into the test solution continuously to ensure complete saturation of the solution.

Brine preparation and solution chemistry characterization: A 3.5 wt.% NaCl brine solution was used for all experiments. The test solution for pure $CO_2$ corrosion experiments was saturated with $CO_2$ for a minimum of 12 hours prior to starting each experiment to reduce oxygen concentration down to 20 ppb, simulating oilfield environments. On the other hand, $N_2$ was used for $H_2S$-containing environment. Prior to commencement of electrochemical measurements for sour corrosion tests, the test samples were initially placed in a $N_2$ saturated brine solution, after which $H_2S$-containing gas mixtures were bubbled into the solution for about 20-30 minutes until in-situ pH stabilizes.   All tests were conducted at atmospheric pressure.

_In-situ electrochemical measurements:_ Electrochemical measurements were conducted on two samples per test cell. Each sample formed the working electrodes in a three electrode cell which also comprised of an Ag/AgCl reference electrode and a platinum auxiliary electrode. Corrosion rate measurements were conducted using DC measurements with an ACM Gill 8[†] potentiostat. Linear Polarization Resistance (LPR) measurements were performed by polarizing the working electrode from ±15 mV about the OCP at a scan rate of 0.25 mV/s to obtain a polarization resistance measurement ($R_p$). Electrochemical impedance spectroscopy (EIS) measurements were performed to determine and compensate for solution resistance and approximate values for each test are presented in Table 3. Tafel polarization measurements were performed using the same potentiostat on freshly polished samples at each experimental condition to determine anodic and cathodic Tafel constants and ultimately the Stern-Geary coefficient, which was subsequently used in conjunction with the measured values of $R_p$ to estimate general corrosion rates. Tafel plots were obtained by performing anodic and cathodic sweeps as two separate sweeps on two different samples in the same test cell, ±250 mV about the OCP at a scan rate of 0.25 mV/s. Both anodic and cathodic sweeps were performed on separate samples to ensure reliable measurements and the cathodic sweep was always performed first.

**Table 3: Solution resistance of solution at different temperature and gas atmosphere**

| Temperature (ºC) | Solution resistance | | |
|---|---|---|---|
| | 100mol.% $CO_2$ (Ohm.cm$^2$) | 10 mol.% $H_2S$ – 90 mol.% $CO_2$ (Ohm.cm$^2$) | 10mol.% $H_2S$ - 90mol.%$N_2$ (Ohm.cm$^2$) |
| 30 | 9.2 | 10.4 | 10.0 |
| 50 | 7.3 | 8.4 | 7.0 |
| 80 | 4.2 | 5.5 | 5.6 |

Characterization of pitting corrosion damage: Corrosion tests were conducted for 7 hours with the aim of investigating the initial film formation of iron sulfide corrosion products and the impact these had on the growth of surface pits. Pit depth measurements were conducted in alignment with ASTM G46-94[(1)21]. An NPFLEX 3D[†] interferometer was used in this study for defining the discrete geometry of pits on almost the entire steel sample surface area. Pits were identified based on carefully chosen thresholds with distinct pit depths, diameters, and areas being quantified. ASTM G46-94 stipulates that an average of the 10 deepest pits and the maximum pit depth (based on relative pit depth measurement after removal of corrosion products) should be

[†] Trade name

[(1)] A.S.T.M. International, _ASTM G46-94 Standard Guide for Examination and Evaluation of Pitting Corrosion_, 2005.

used for pit damage characterization for the sample area. A sample surface area of 9 x 9 mm$^2$ was analyzed for pits from the 10 x 10 mm$^2$ sample. A systematic stitching approach is adopted whereby 9 different 3 x 3 mm$^2$ areas are stitched together.

It is very important to note here that there is no generally accepted consensus on the minimum dimensions a pit can take in terms of depth and diameter, especially in non-passivating alloys like carbon steels. However, there are various suggestions of the different possible shapes, orientations and sizes of pits in the ASTM G46-94[21]. Nonetheless, visual evidence of pits/cavities in terms of the maximum pits identified by the techniques implemented in this work is provided later within this paper.

## RESULTS AND DISCUSSION

<u>Tafel plot and electrochemical observations:</u> Figure 1 shows the Tafel plots obtained at the end of the test by performing separate anodic and cathodic sweeps ±250 mV about the OCP of UNS K03014 carbon steel at a scan rate of 0.25 mV/s after 7 hours of immersion in the test solution. The graphs correspond to solutions at temperatures of 30, 50 and 80°C. Repeatable Tafel polarization test results were carried out after monitoring the corrosion rates from LPR measurements for 7 hours. Corrosion rate in this instance was found to be exactly the same as the corrosion rates presented in Figures 2, 4 and 6 in separate tests. Table 5 indicates the measured Tafel constants and the resulting Stern-Geary coefficient for all test conditions. Each respective value of Stern-Geary coefficient was used with the polarization resistance ($R_p$) to determine corrosion rate as a function of time. The repeatability of the Tafel polarization curves was also confirmed by comparing corrosion rate from Tafel extrapolation with estimated corrosion rate from linear polarization measurements after 7 hours. This is provided in Table 6.

In order to fully appreciate the effect of $H_2S$ in this work, it is important to afford consideration to the complex cathodic reaction mechanisms that defines the term "$CO_2$ corrosion" as emphasized by Dugstad[22]. At lower pH and in an un-buffered system as is the case of this work, both the $H^+$ reduction reaction and direct reduction of $H_2CO_3$ will contribute to the total cathodic current[23]. Consequently, the cathodic currents represented in the Tafel polarization plots presented in Figure 1 for pure $CO_2$ corrosion environments represent the collective influence of $H^+$ reduction and $H_2CO_3$ reduction reactions (and water reduction and low potential). It has also been shown by Nesic et al.[23] that the $H^+$ reduction reaction becomes less dominant with increasing pH.

**Table 4: Average measured in-situ pH of test solutions-gas systems for the first 7 Hours**

| Temperature (ºC) | In-situ pH of test solutions | | |
|---|---|---|---|
| | 100% $CO_2$ | 10mol.% $H_2S$ - 90mol.% $CO_2$ | 10mol.% $H_2S$ - 90mol.% $N_2$ |
| 30 | 4.0 ± 0.2 | 4.3 ± 0.01 | 4.7 ±0.01 |
| 50 | 4.1 ± 0.2 | 4.1 ± 0.1 | 4.6 ± 0.1 |
| 80 | 4.3 ± 0.3 | 4.4 ± 0.1 | 4.8 ±0.1 |

**Table 5: Tafel constants at different temperatures and gas mixtures**

| Temperature (ºC) | Mole % of combining gases | | | | | | | | |
|---|---|---|---|---|---|---|---|---|---|
| | 100mol.% $CO_2$ | | | 10mol.% $H_2S$-90mol.% $CO_2$ | | | 10mol.% $H_2S$-90mol.% $N_2$ | | |
| | $\beta_a$ | $\beta_c$ | B | $\beta_a$ | $\beta_c$ | B | $\beta_a$ | $\beta_c$ | B |
| 30 | 32.5 | 200 | 12.14 | 35 | 140 | 12.16 | 55 | 170 | 18.04 |
| 50 | 40 | 168 | 14.03 | 45 | 140 | 14.79 | 57.5 | 140 | 17.70 |
| 80 | 57.5 | 135 | 17.51 | 57.5 | 160 | 18.37 | 47 | 135 | 15.14 |

**Table 6: Comparison between corrosion rates (mm/yr) obtained from Tafel extrapolation and from the use of the estimated Stern-Geary constants**.

| Temperature (ºC) | Corrosion rate (mm/yr) after 7 hours | | | | | |
|---|---|---|---|---|---|---|
| | 100mol.% $CO_2$ | | 10mol.% $H_2S$ - 90mol.% $CO_2$ | | 10mol.% $H_2S$ - 90mol.% $N_2$ | |
| | CR-LPR | CR-Tafel | CR-LPR | CR-Tafel | CR-LPR | CR-Tafel |
| 30 | 1.05 | 1.19 | 0.41 | 0.39 | 0.26 | 0.29 |
| 50 | 2.10 | 2.58 | 1.02 | 0.95 | 0.56 | 0.55 |
| 80 | 4.77 | 5.23 | 1.44 | 1.25 | 0.59 | 0.63 |

Tafel plots within Figure 1 suggest that the presence of 10 mol. %$H_2S$ gas, in the $CO_2$ gas phase, influences both the anodic and cathodic reactions at all temperatures. However, its influence on the cathodic reaction is more significant than on the anodic reaction. There is a shift from a cathodic process significantly controlled by mass-transfer in completely sweet environment to an activation controlled cathodic reaction in $H_2S$-containing environment. This shift has been attributed to the suppression of the collective influence of $H^+$ and $H_2CO_3$ reduction reaction[17,24] that dominates the cathodic current in sweet corrosion environment even with the addition of 0.65% of $H_2S$. There is also the addition of a direct or heterogeneous cathodic reduction reaction of $HS^-$ [18,24], especially at higher concentration of $H_2S$ gas in the gas phase, as is the case in this work. The shift from mass transfer influenced cathodic process in sweet corrosion environment to activation-controlled in $H_2S$-containing environment becomes more apparent with decreasing temperature.



(a)



(b)
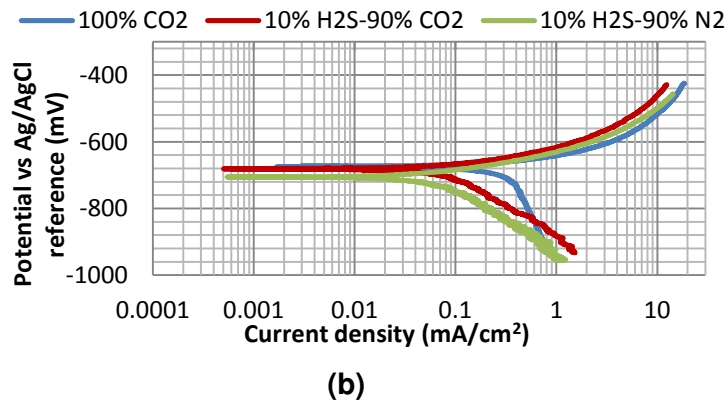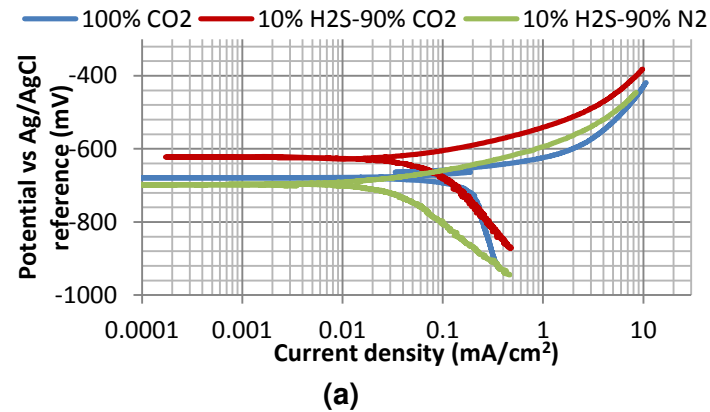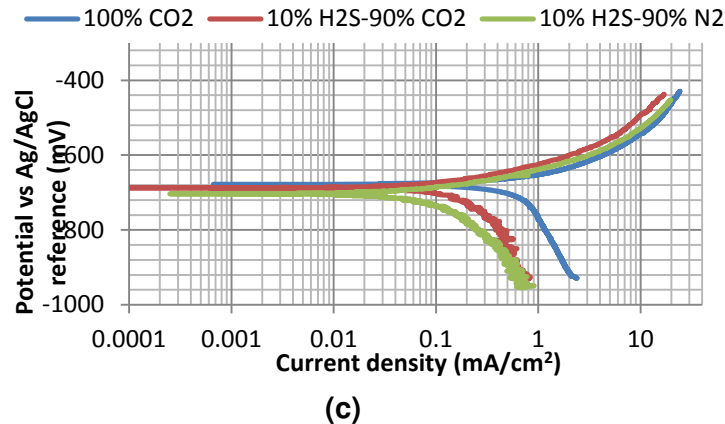
**Figure 1.** Tafel polarization plots for UNS K03014 carbon steel in 3.5 wt.% NaCl solution saturated with 100 mol.% CO2, 10 mol.% H2S- 90 mol.%CO2 and 10 mol.% H2S-90 mol.% N2 at (a) 30 °C, (b) 50 °C and (c) 80 °C.

This behavior suggests that there is still a significant contribution of $H_2CO_3/H^+$ reduction reactions to the total cathodic current with a shift from completely sweet corrosion scenario to sour corrosion scenario. This has also been confirmed by Kittel et al.[24] for experiments carried out using 316 stainless steel. The contribution of $H_2CO_3/H^+$ reduction reactions to cathodic current appears to increase with temperature for systems containing 10 mol.% $H_2S$ – 90 mol.% $CO_2$. It is also expected that the un-buffered pH of the test solutions may vary slightly for the three gas systems under investigation as provided in Table 4. Thus it would be expected that the pH and hence $H^+$ reduction reaction may become significant to varying degree for the different experimental conditions. While Zheng et al.[17] had reported that the main contribution to the cathodic current at 10% $H_2S$ concentration is from the direct reduction of aqueous $H_2S$ species, it can also be argued from results shown in Figure 1 that the corrosion reaction of steel with $H_2S$ in $H_2S$-containing environments dominates the reaction mechanism at lower temperature and becomes less dominant as the temperature increases  and that the $H^+$ reduction mechanism which is strongly influenced by solution pH (and $H^+$ concentration) is not as influential

Corrosion rate and corrosion products at 30ºC:

The corrosion rate measurements at 30ºC for test solutions saturated with 100 mol. % $CO_2$ gas, 10 mol. % $H_2S$ – 90 mol. % $CO_2$ gas mixture and 10 mol. % $H_2S$ – 90 mol. % $N_2$ gas mixtures for 7 hours are presented in Figure 2. The corrosion rate is constant for the three different gas systems. However, with 100 mol. % $CO_2$ in the gas phase, the corrosion rate is three times higher than a gas phase composition of 10 mol. % $H_2S$ – 90 mol. % $CO_2$ gas and four times higher than a gas phase composition of 10 mol. % $H_2S$ – 90 mol. % $N_2$. There was no significant difference between corrosion rate of carbon steel with a gas phase of 10 mol. % $H_2S$ – 90 mol. % $CO_2$ gas mixture and 10 mol. % $H_2S$ – 90 mol. % $N_2$. This correlates well with the Tafel polarization plot of Figure 1(a) as well as observations by other authors[14, 17].

It also suggests that reduction reactions associated with $H_2S$ dominate the cathodic current at 30ºC as observed by Zheng et al.[17] at pH of 4. Since the pH for 10 mol. % $H_2S$ – 90 mol. % $CO_2$ is always slightly lower than for 10 mol. % $H_2S$ – 90 mol. % $N_2$ (Table 4), It can therefore be inferred that $H_2S/HS^-$ reduction dominates the cathodic reaction mechanisms in $H_2S$-containing systems.  While Zheng et al.[17] observed a slight drop in corrosion rate from ~1.8 mm/yr in 100% $CO_2$ system to ~1.2 mm/yr in 10 mol. % $H_2S$ – 90 mol. % $CO_2$ at 30ºC, pH of 5, rotating speed of 1000rpm and after 2 hours, results by Ma et.al[14] confirmed that with increased exposure time,

the formation of an iron sulfide corrosion layer would reduce the corrosion rates similar to those presented in Figure 2.
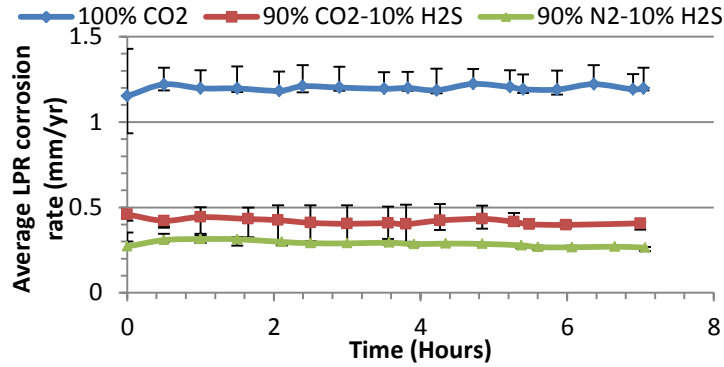


**Figure 2. Corrosion rate of UNS K03014 carbon steel in 3.5 wt.% NaCl solution saturated with gas streams of different composition at 30ºC.**



(a)



FeS film covered area
(Via EDX point analysis and XRD)

(b)



FeS film covered area
(Via EDX point analysis and XRD)

(c)



(d)
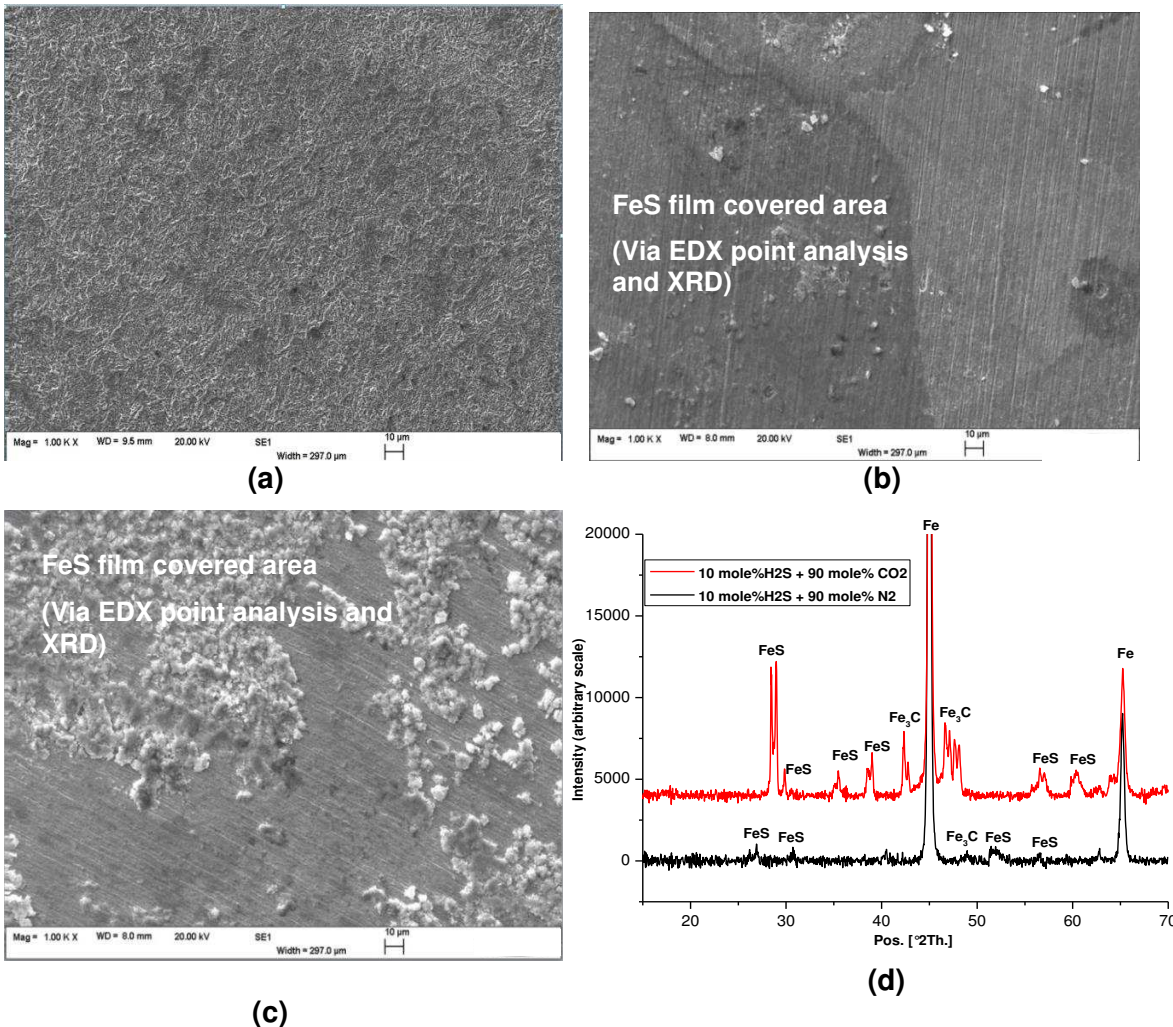
**Figure 3: SEM images of corrosion product layer on UNS K03014 carbon steel in 3.5 wt. % NaCl solution saturated with (a) 100 mol. % $CO_2$, (b) 10 mol. % $H_2S$- 90 mol. %$CO_2$ and (c) 10 mol. % $H_2S$-90 mol. % $N_2$ at 30 ℃. (d) XRD pattern for corrosion product layer on UNS K03014 carbon steel in 3.5 wt.% NaCl solution saturated 10 mol. % $H_2S$- 90 mol. %$CO_2$ and 10 mol. % $H_2S$-90 mol. % $N_2$ at 30 ℃. Images are for test duration of 7 hours. _(Note that the intensity scale is arbitrary)_.**

So much of reduction effect has either been attributed to the suppression of the collective contribution of $H^+$ and $H_2CO_3$ reduction reaction due to the presence of $H_2S$ gas by Zheng et al.[17], or to the formation of iron sulfide corrosion products (most likely mackinawite) by other authors[9,14]. The latter is known to be a "kinetically-favored" phase of iron sulfide[9]. Figures 3(a), (b), and (c), shows the SEM images of corrosion product layer for gas phase composition of 100 mol. % $CO_2$, 10 mol. % $H_2S$ – 90 mol. % $CO_2$ and 10 mol. % $H_2S$ – 90 mol. % $N_2$ at (a) 30°C at the end of test in Figure 2 respectively. From SEM images of Figure 3(a), the corrosion product layer on steel is not surprisingly mainly empty cementite for a gas system composed of only $CO_2$ gas. However, Figure 3(b) and (c) show the presence of a very thin non-crystalline and a "smudge-like textured' iron sulfide corrosion product layer with a non-uniform coverage for gas systems composed of 10 mol. % $H_2S$ – 90 mol. % $CO_2$ and 10 mol. % $H_2S$ – 90 mol. % $N_2$, respectively. The corrosion product layer on carbon steel exposed to gas systems composed of 10 mol. % $H_2S$ – 90 mol. % $CO_2$ and 10 mol. % $H_2S$ – 90 mol. % $N_2$ has been confirmed to be iron sulfide films from EDX analysis and the XRD pattern provided in Figure 3(d). Although it is apparent that the film morphology in both gaseous systems are physically different, it is still not clear if the presence of, or absence of $CO_2$ gas in the gaseous phase is the cause of this difference, especially as the presence of, or absence of $CO_2$ gas appears to have a slight influence on the solution pH of the test solutions in $H_2S$-containing environments (Table 4).

Corrosion rate and corrosion products at 50ºC

The corrosion rate of carbon steel in the test solution shown in Figure 4 depicts a distinctive difference in magnitude for the gas systems used in this work. The results show that highest corrosion rate values were recorded with a gas phase composed of only $CO_2$. This was almost three times higher than a gas system composed of 10 mol. % $H_2S$ – 90 mol. % $CO_2$ and 10 mol. % $H_2S$ – 90 mol. % $N_2$ at the start of the experiment. While this trend appears different from the results published by Zheng et al.[17] for test at 30ºC, the easily noticed disparity in the magnitude of corrosion rate among the three gas systems, increases with time. This suggests that with increase in temperature, the combined $H^+$ and $H_2CO_3$ reduction reactions become increasingly influential. This can easily be related to the Arrhenius-type dependence of $CO_2$ corrosion on temperature [23,25].
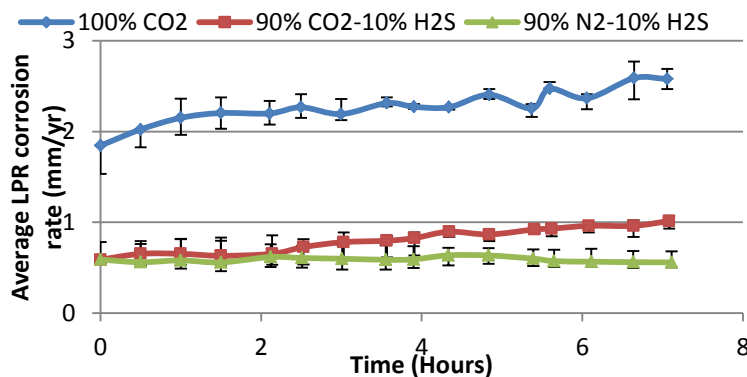


**Figure 4: Corrosion rate of UNS K03014 carbon steel in 3.5 wt.% NaCl solution saturated with gas streams of different composition at 50ºC.**

The SEM images shown in Figure 5 confirms the existence of an empty cementite network as the main corrosion product layer with 100 mol. % $CO_2$ in the gas phase and a corrosion product layer of iron sulfide when the gas phase composed of 10 mol. % $H_2S$ – 90 mol. % $CO_2$ gas and 10 mol. % $H_2S$ – 90 mol. % $N_2$. The iron sulfide layer at 50ºC is quite obvious with stronger signal for Iron sulfide on the XRD (Figure 5(d)). The morphology of the iron sulfide films are also quite different for 10 mol. % $H_2S$ – 90 mol. % $CO_2$ gas and 10 mol. % $H_2S$ – 90 mol. % $N_2$ gas

combination. There was also observation of delamination of the iron sulfide film in Figure 5(b) which is similar to the findings of other authors such as Brown and Nesic [20].
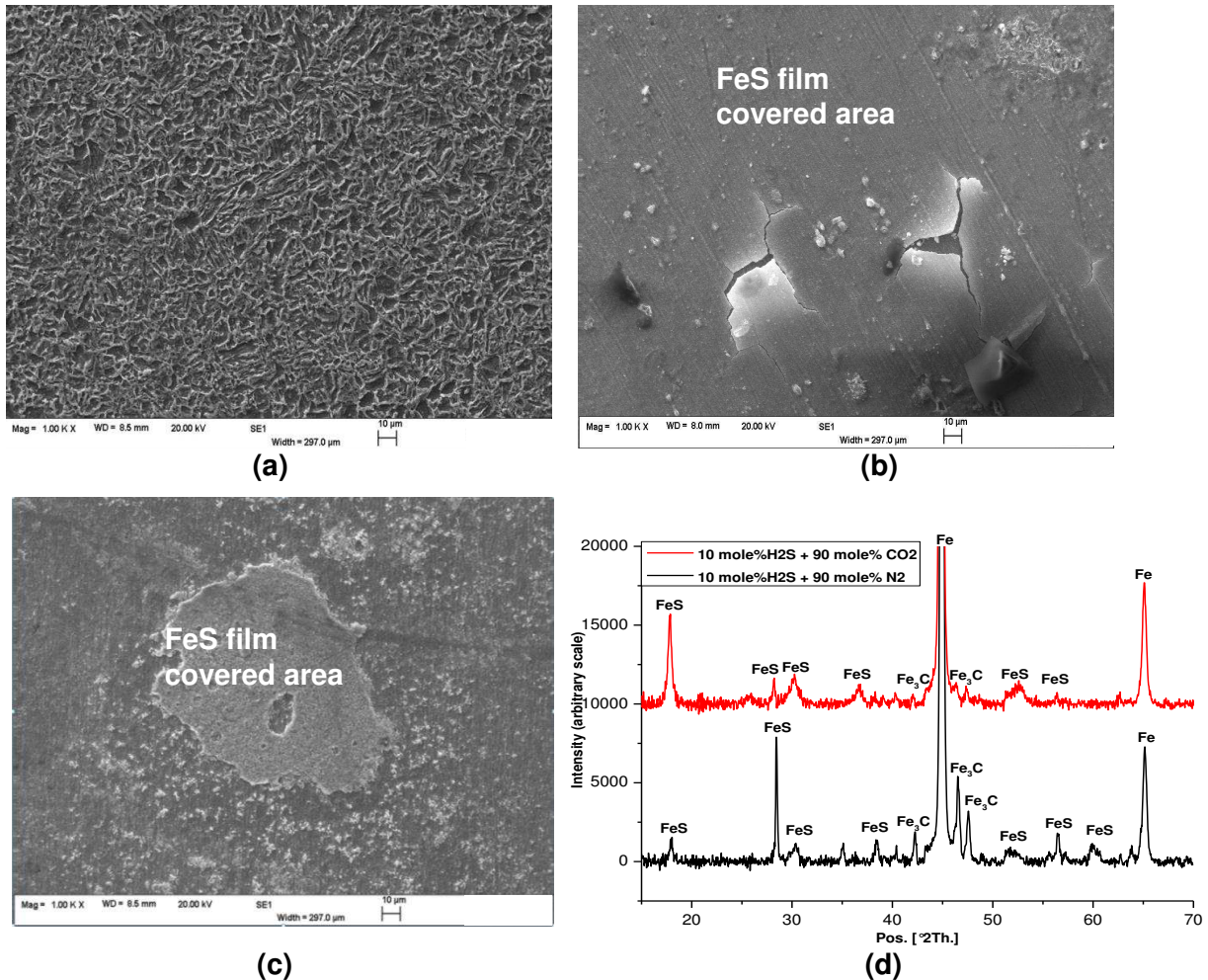


**Figure 5: SEM images of corrosion product layer on UNS K03014 carbon steel in 3.5 wt. % NaCl solution saturated with (a) 100 mol. % CO$_2$, (b) 10 mol. % H$_2$S- 90 mol. %CO$_2$ and (c) 10 mol. % H$_2$S-90 mol. % N$_2$ at 50 ℃. (d) XRD pattern for corrosion product layer on UNS K03014 carbon steel in 3.5 wt.% NaCl solution saturated 10 mol. % H$_2$S- 90 mol. %CO$_2$ and 10 mol. % H$_2$S-90 mol. % N$_2$ at 50 ℃. Images are for test duration of 7 hours. *(Note that the intensity scale is arbitrary)*.**

Corrosion rate and corrosion products at 80ºC:

The corrosion rate of carbon steel in brine saturated with the three different gas combinations at 80ºC is given in Figure 6. The difference in corrosion rate over the duration of the test is consistent with the behavior observed at 50ºC.  At 80ºC, the contribution of the H$^+$ and H$_2$CO$_3$ reduction reactions to total cathodic current in 10 mol. % H$_2$S – 90 mol. % CO$_2$ containing atmosphere appears to be more significant than at lower temperatures. This also correlates well with the observation from potentiodynamic sweep (Figure 1(c)). Such observation at 80ºC is an indication for the potential increased contribution from uniform corrosion to total material penetration. There is also marginally enhanced contribution from cumulative uniform corrosion to total metal penetration at 80ºC for 10 mol. % H$_2$S – 90 mol. % N$_2$ gas systems than at 50ºC. However, the uniform corrosion contribution was relatively higher for 10 mol. % H$_2$S – 90 mol. % CO$_2$ gas system due to the presence of CO$_2$ gas in the gas phase. It is believed that the

significant increase in corrosion rate at 80ºC when compared to 30 and 50ºC could be linked to the combined effect of $H^+$ and $H_2CO_3$ reduction reactions to the corrosion process.
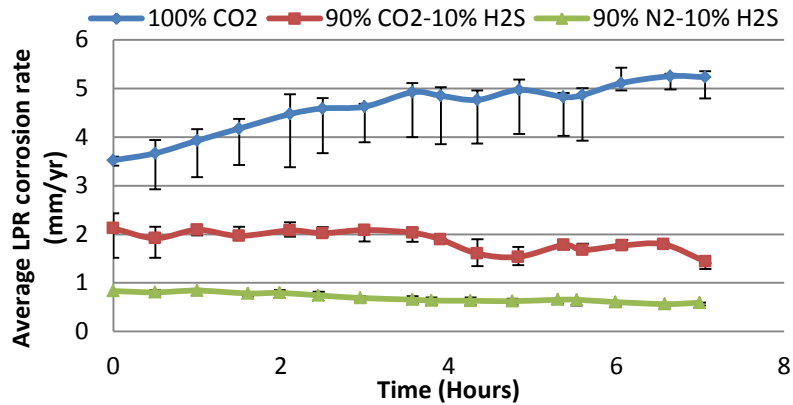


**Figure 6: Corrosion rate of UNS K03014 carbon steel in 3.5 wt.% NaCl solution saturated with gas streams of different composition at 80ºC.**
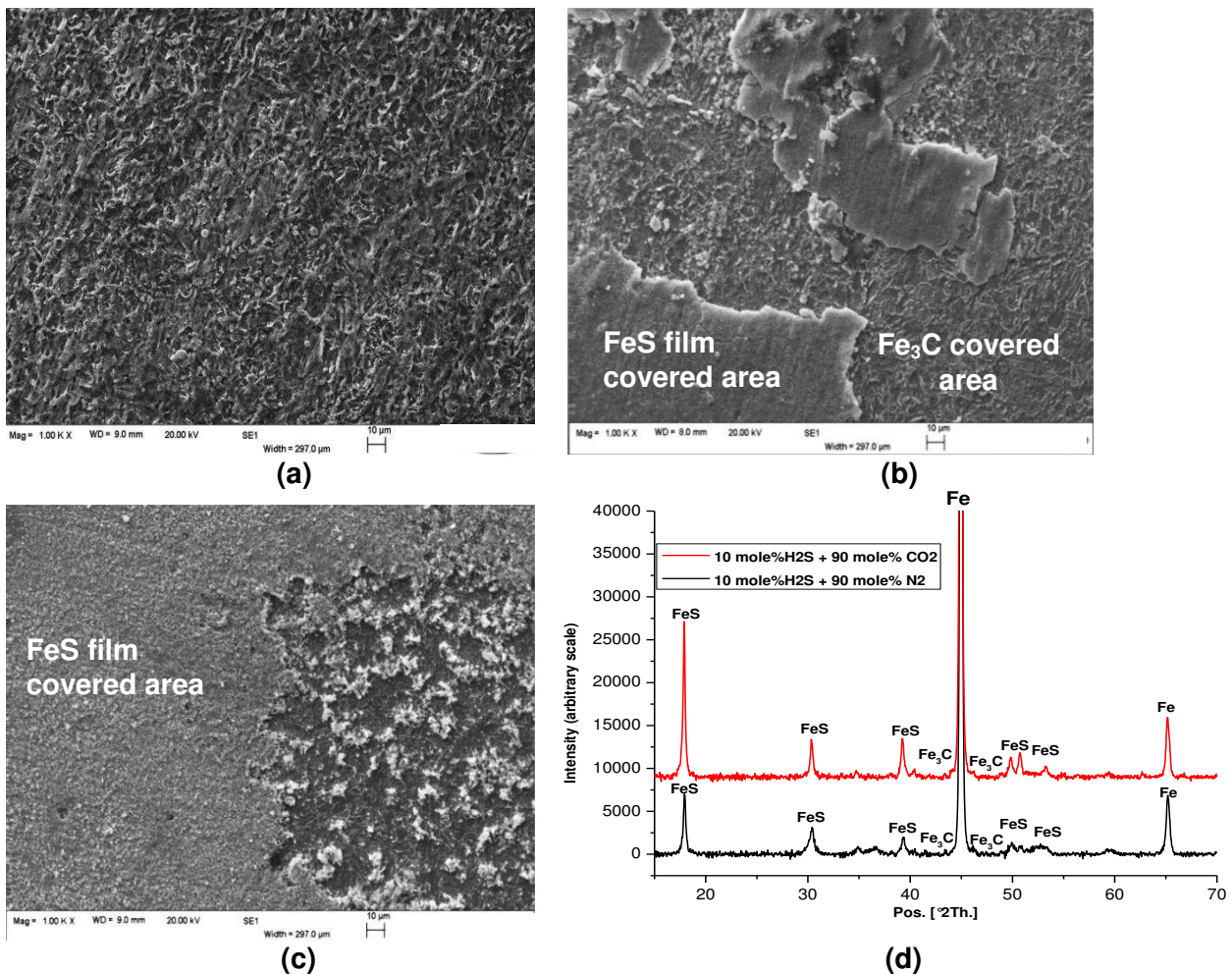


**Figure 7: SEM images of corrosion product layer on UNS K03014 carbon steel in 3.5 wt. % NaCl solution saturated with (a) 100 mol. % $CO_2$, (b) 10 mol. % $H_2S$- 90 mol. %$CO_2$ and (c) 10 mol. % $H_2S$-90 mol. % $N_2$ at 80℃. (d) XRD pattern for corrosion product layer on UNS K03014 carbon steel in 3.5 wt.% NaCl solution saturated 10 mol. % $H_2S$- 90 mol. %$CO_2$ and 10 mol. % $H_2S$-90 mol. % $N_2$ at 80℃. Images are for test duration of 7 hours. *(Note that the intensity scale is arbitrary).***

What remains unclear thus far is the extent to which the temperature changes could be influencing the kinetics of iron sulfide formation. A slight indication of such effect can be seen on the SEM images of Figure 7((a) – (c)) and the corresponding XRD pattern (Figure 7(d). The empty cementite network of Figure 7(a) for the test containing only $CO_2$ gas corresponds to what has been initially reported to contain only traces of a non-crystalline forms of iron carbonate corrosion products at 80ºC[7]. However, the iron sulfide corrosion product layer appears to be a continuous layer with heavily corroded localized regions, showing empty cementite with the test containing 10 mol. % $H_2S$ – 90 mol. % $CO_2$ gas. When the system is saturated with 10 mol. % $H_2S$ – 90 mol. % $N_2$, the corrosion product morphology is quite different from the former and shows evidence of less corrosion of surrounding regions without the iron sulfide films. This could be related to the absence of $CO_2$ gas as well as the combined effect of $H^+$ and $H_2CO_3$ reduction reactions to the corrosion process. The peaks of the XRD pattern confirm the formation of Iron sulfide.

Pitting corrosion initiation in sweet and sour corrosion systems: The main focus of this research is to assess the initiation and/or propagation of pitting corrosion of carbon steel material in sour corrosion environments with respect to sweet corrosion environments. Figures 8 present the maximum and average pit depth of almost the entire exposed surface of the samples (relative to the corroded surface after removal of corrosion products) respectively. The average pit depth represents an average of the 10 deepest pits as stipulated by ASTM G46-94 [21]. Referring to Figures 10 and 11, at the end of the 7 hours, there were no pits on the test sample at 30ºC in a test atmosphere composed of 100mol.% $CO_2$. In this same gas atmosphere, the maximum pit depth on the surface also increases to a maximum at 50ºC and then decreases slightly at 80ºC. Similar behavior with temperature change has previously been reported [7] in separate tests.
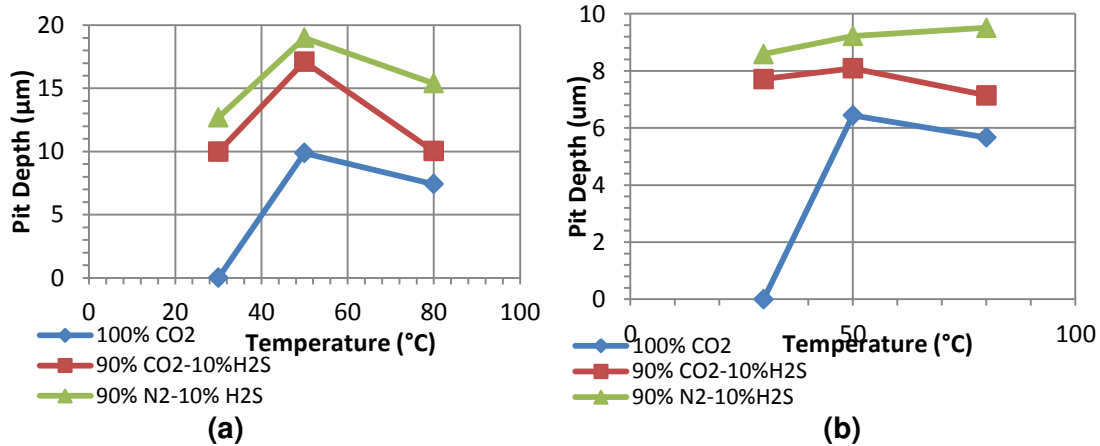


Figure 8: (a)Maximum pit depth (relative to corroded surface) and (b) Average pit depth (relative to corroded surface) on UNS K03014 carbon steel surface exposed to corrosion system under 100mol. % $CO_2$, 10mol. % $H_2S$ - 90mol. % $CO_2$ and 10mol. % $H_2S$ - 90mol. % $N_2$ gas atmosphere as a function of temperature.

The initial increase in pit depth from 30 to 50ºC was attributed to the effect of temperature on the kinetics of corrosion and the rate of revealing of empty cementite. Empty cementite has been linked to potential galvanic effect ultimately leading to pitting/localized corrosion[2,7,26]. However, the slight decrease in pit depth at 80ºC is due to the extensive uniform corrosion of surround surfaces [7]. Examples of the maximum pit depth identified in $H_2S$-$CO_2$ containing gas atmosphere are provided in Figure 9 as visual evidence of measurable pits. In the 10mol. % $H_2S$ - 90mol. % $CO_2$ and 10mol. % $H_2S$ - 90mol. % $N_2$ gas atmosphere, the results in Figure 8 also shows that the pit depth increases from a gas atmosphere of 100 mol. % $CO_2$, to 10mol. % $H_2S$

- 90mol. % $CO_2$, and 10mol. % $H_2S$ - 90mol. % $N_2$, while at the same time the general corrosion rate increases in the reverse direction.



(a)

(b)

(c)
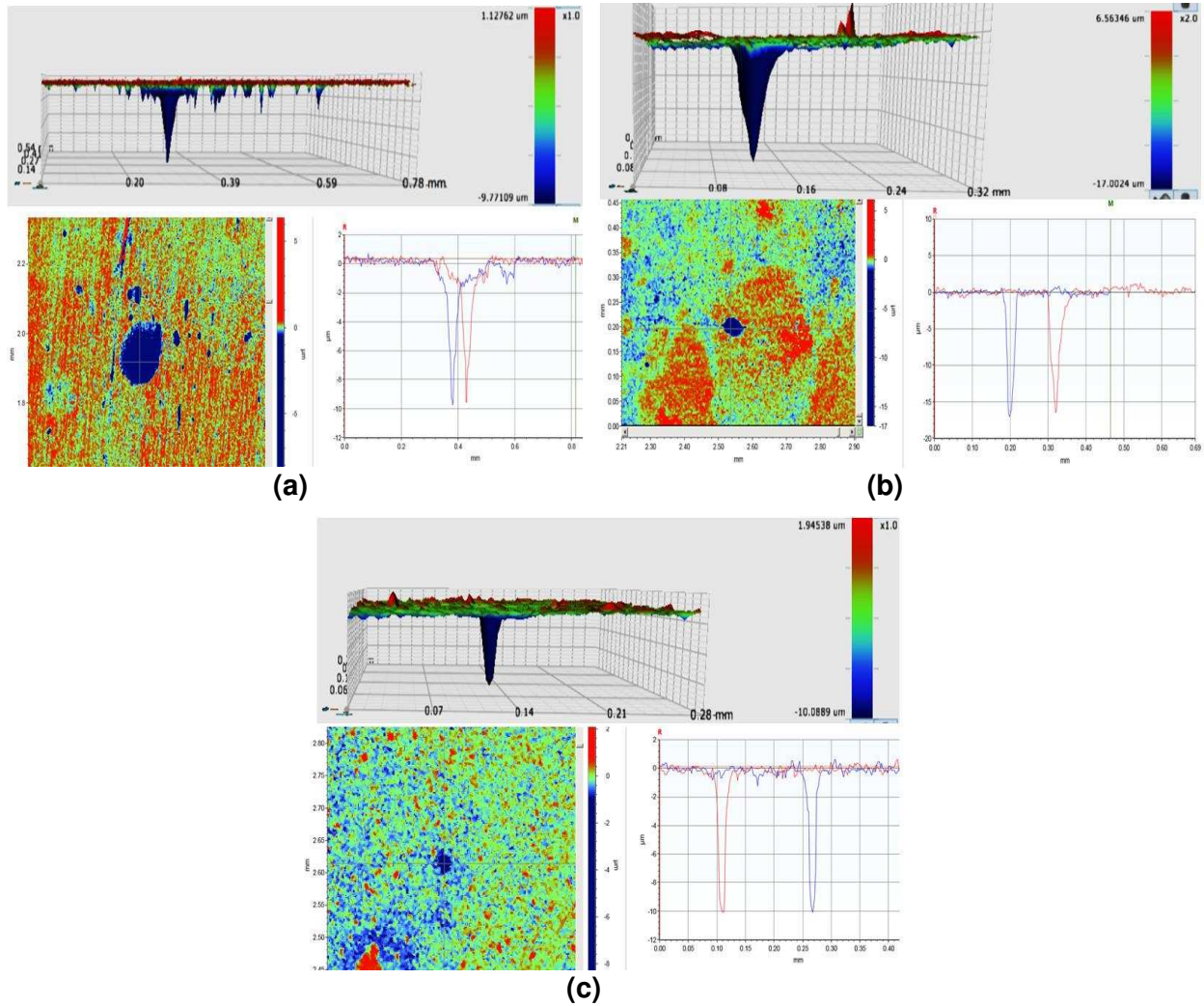
**Figure 9: 2D and 3D images of Deepest pit (relative to corroded surface) on UNS K03014 carbon steel surface exposed to corrosion system under 10mole% $H_2S$ - 90mole% $CO_2$ for 7 hours at (a) 30ºC, (b) 50ºC, and (c) 80ºC.**

This was observed to be similar for all temperatures. However, the trend of change in pit depth with changing temperature was the same for all gas combinations. This suggests that $CO_2$ corrosion rate manifests mainly in the form of uniform corrosion in an un-buffered test system.

It is also important to recognize that the significant pitting or propensity for pit to initiate in 10mol. % $H_2S$ - 90mol. % $CO_2$ and 10mol. % $H_2S$ - 90mol. % $N_2$ gas atmosphere is much related to the formation of iron sulfide films. These films have been confirmed to be mainly makinawite using the XRD pattern of 3(d), 5(d) and 7(d) and literature data [27,28]. Pitting corrosion as observed in this work and in $H_2S$ containing gas atmosphere has also been reported by other authors [20]. However, it has clearly been shown here that the presence of $H_2S$ gas and formation of iron sulfide (mackinawite) are the main agents for pit initiation and that the presence of $CO_2$ may increase total material loss due to the $CO_2$ corrosion contribution, but minimise the extent of pitting. However, the contribution of $CO_2$ corrosion to material loss has been shown to be supressed by low levels of $H_2S$ gas and much more lower than levels used in this work[16,17].

<u>The concept of total metal penetration and pitting factor:</u> The concept of total metal penetration has been introduced in previous publication[7] as a useful tool for characterising the corrosion damage morphology in of carbon steel in environment where the steel is predesposed to both piting and uniform corrosion. When considering the threat posed to carbon steel pipework subject to the prospect of pitting corrosion, the potential failure of a pipeline will always depend not only upon the rate at which pits propagate *relative* to the corroding surface, but also on the uniform corrosion rate of the surrounding area. Refering to Figure 10, the change in total penetration depth (i.e. uniform thickness plus pit depth relative to the corroded surface) as a function of temperature can be observed for each of the three gas systems used in this work. The results indicate that due to the substantial general corrosion rate of the sample exposed to solution in 100mol.% $CO_2$ gas atmosphere, the total thickness loss or total penetration depth far exceeds that of the samples exposed to the solution under 10mol. % $H_2S$ - 90mol. % $CO_2$ gas and 10mol. % $H_2S$ - 90mol. % $N_2$ gas atmophere, where the uniform thickness loss is negligible in comparison to the pit depth relative to corroded surface. The uniform corrosion contribution to total metal penetration also increases with temperature and $CO_2$ content in the gas phase.
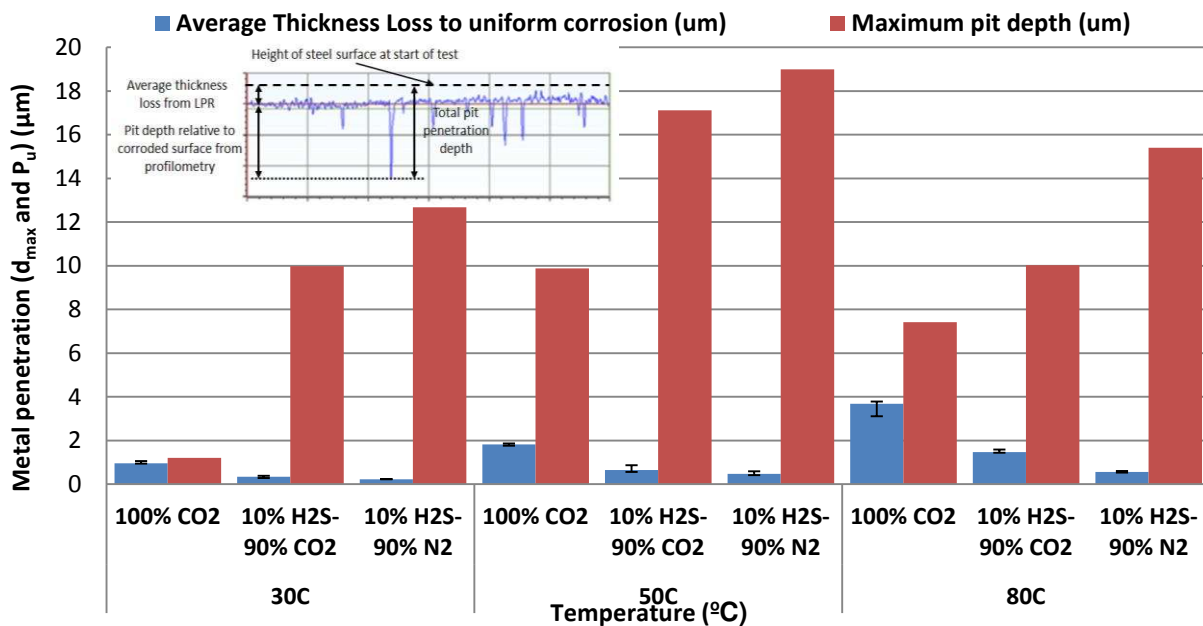


**Figure 10: Total pit penetration on UNS K03014 carbon steel surface exposed to corrosion system under 100mol. % $CO_2$, 10mol.% $H_2S$ - 90mol. % $CO_2$ and 10mol.% $H_2S$ - 90mol. % $N_2$ gas atmosphere as a fuunction of temperature indicating the contribution of general thickness loss (from LPR) and pit depth relative to corroded surface (determined from surface profilometry)**

It could be considered that the high general corrosion rate observed at 80ºC and in 100mol. % $CO_2$ gas atmopshere has the ability to essentially mask pit growth. However, the uniform corrosion contribution reduces significantly with the presence of $H_2S$ gas, but still higher than at 50ºC. This suggests that at 80ºC, there is significant protection from iron sulfide that must have reduced both pitting and uniform corrosion. The mechanism by which this may be occurring remains unclear, but could be related to the contribution of iron sulfide formation from the aqueous corrosion reaction mechanism as suggested by other authors[9-11]. It could be imagined that the higher rate of metal dissolution at the start of the experiment at 80ºC could be favouring the kinetics of iron sulfide formation in the corrosion interface.

Theoretically, metal penetration is occuring at a faster rate than that identified from purely the profilometry depth measurements relative to the corroding surface. Affording consideration to the uniform corrosion rate of the surrounding area is a fundamental consideration when

reviewing the susceptibility of the carbon steel to pitting corrosion when the general corrosion rate is appreciable. For tests performed under 10mol. % $H_2S$ - 90mol. % $CO_2$ gas and 10mol. % $H_2S$ - 90mol. % $N_2$ gas atmophere, initiation of pit is not significantly masked by the general corrosion rate. The results shown in Figure 10 also suggest that the presence of $H_2S$ gas in the gas atmopshere is reducing the general corrosion rate, but not necessarily reducing the risk of pitting of carbon steel pipelines.

Pitting Factor: The concept of pitting factor ($P_f$) has been introduced as a tool for characterization of the nature of corrosion damage in this work. The pitting factor is used to reflect the relative contribution of corrosion damage mechanism (between uniform and pitting corrosion) at each experimental sampling time and is defined in ASTM G46-94 [21] as:

$$P_f = (\frac{P_d}{P_u}) \tag{3}$$

Where $P_d$ is the deepest metal penetration (µm) for the whole exposed surface area (sum of maximum pit depth ($d_{max}$) (after removal of corrosion products) plus the average metal penetration (µm) from general corrosion rate measurement (termed $P_u$), i.e; $P_d = P_u + d_{max}$. A pitting factor of 1 represents uniform corrosion. The greater the pitting factor, the greater the depth of penetration relative to the surrounding surface area.

The pitting factor analysis presented in Figure 11 are a clear indication that the corrosion damage mechanism observed in test solution under the 100mol. % $CO_2$ gas atmosphere is actually pitting even while there is still substantial uniform corrosion taking place. Under a gas atmosphere of 10mol. % $H_2S$ - 90mol. % $CO_2$ gas and 10mol. % $H_2S$ - 90mol. % $N_2$, the pitting factor was higher and decreases with temperature because of the effect of uniform corrosion of the surrounding surface. This suggests that pit initiation occurs and dominates the corrosion damage mechanism in sour corrosion environment once iron sulfide is formed. The pitting factor of carbon steel under a purely $CO_2$ corrosion atmosphere confirms that there was very significant general corrosion.
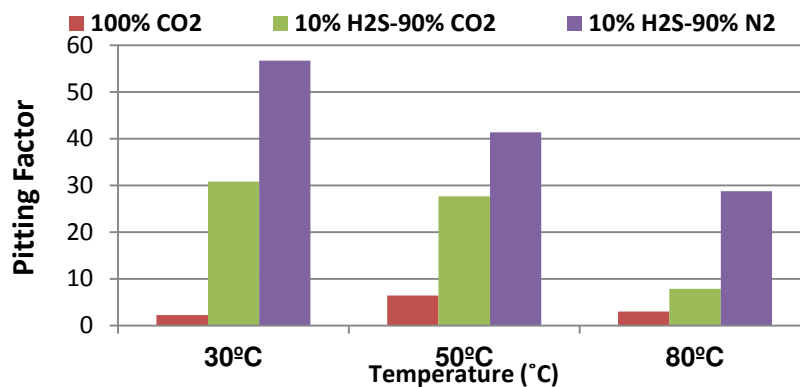


**Figure 11: Variation of pitting factor for UNS K03014 carbon steel surface exposed to corrosion system under 100mole% $CO_2$, 10mole% $H_2S$ - 90mole% $CO_2$ and 10mole% $H_2S$ - 90mole% $N_2$ gas atmosphere as a function of temperature.**

## CONCLUSION

The corrosion behavior of carbon steel material in $CO_2$ and $H_2S$ containing brine has been investigated at three different temperatures and with emphasis on iron sulfide film formation, uniform corrosion and pit initiation. The following conclusions were deduced from the results of this work.

- In pure $CO_2$ corrosion systems, uniform corrosion was dominant, which tends to mask the true extent of total material penetration, especially at higher temperatures.

- The presence of $H_2S$ in the gas phase appears to be having a two pronged effect on corrosion behavior of carbon steel.

  1) Supressing the combined contribution of $CO_2/H_2CO_3$ and/or $H^+$ reduction reaction to total cathodic current and hence producing a lower corrosion rate of steel. The former is correlated on the slight influence of $H_2S$ on the pH in $CO_2$-$H_2S$ systems.

  2) The very fast process of formation of iron sulfide films from direct reduction reaction of $H_2S/HS^-$ and acting as the precursor for more pitting in tests under 10mol. % $H_2S$ - 90mol. % $CO_2$ gas and 10mol. % $H_2S$ - 90mol. % $N_2$ gas atmosphere when compared to tests in pure $CO_2$ systems.

- The effect of $H_2S$ gas on reducing the corrosion rate (by magnitude) of carbon steel material becomes significant with increase in temperature for tests under 10mol. % $H_2S$ - 90mol. % $CO_2$ gas and 10mol. % $H_2S$ - 90mol. % $N_2$ gas.

- The contribution of $H^+/HCO_3^-$ reduction to cathodic current and overall corrosion rate (by magnitude) in $H_2S$-$CO_2$–containing environment also becomes dominant with increasing temperature.

- Pits initiate quickly in $H_2S$ containing environments than in only $CO_2$-containing environments. For all temperatures, the recorded pit depth was higher in sour gas systems without $CO_2$ gas. This is strongly related to the formation of iron sulfide films as well as the fact that the presence of $CO_2$ gas could be increasing the uniform corrosion contribution to material loss and hence masking the true extent of metal penetration. This is more significant at higher temperatures.

### REFERENCES

1. M.B. Kermani and D. Harrop, "The Impact of Corrosion on Oil and Gas Industry", SPE Production & Operations, 11, 3 (1996): p. 186-190.
2. B. Kermani.M and A. Morshed, "Carbon dioxide corrosion in oil and gas production: A compendium", Corrosion, 59, 08 (2003).
3. B. Hedges, H.J. Chen, K. Sprague, and T.H. Bieri. "A review of monitoring and inspection techniques for $CO_2$ and $H_2S$ corrosion in oil & gas production facilities", CORROSION, paper no, 120, (San Diego, CA:NACE International, 2006).
4. G. Wilken. "Effect of environmental factors on downhole sour gas corrosion", CORROSION, paper no. 76, (Denver, CO: NACE International, 1996).
5. B. Kermani. "Materials optimization for oil and gas sour production", CORROSION, paper no. 156, (Orlando, FL: NACE International, 2000).
6. A. Hernández-Espejel, M.A. Domínguez-Crespo, R. Cabrera-Sierra, C. Rodríguez-Meneses, and E.M. Arce-Estrada, "Investigations of corrosion films formed on API-X52 pipeline steel in acid sour media", Corrosion Science, 52, 7 (2010): p. 2258-2267.
7. F. Pessu, R. Barker, and A. Neville. "Understanding pitting corrosion behaviour of X-65 (UNS K03014) carbon steel in $CO_2$ saturated environments: The temperature effect", CORROSION, paper no. 4214, (San Antonio, TX:NACE International, 2014).
8. S.N.Smith, B.Brown, and W.Sun."Corrosion at higher $H_2S$ concentrations and moderate temperatures",CORROSION, paper no.81, (Houston,TX:NACE International, 2011).

9. W. Sun, D. V.Pugh, S. N.Smith, S. Ling, J. L.Pacheco, and R. J.Franco. "A parametric study of sour corrosion of carbon steel ", CORROSION, paper no.278, (San Antonio, TX:NACE International, 2010).

10. S. Nesic, H. Li, J. Huang, and D. Sormaz. "An open source mechanistic model for CO2 / H2S corrosion of carbon steel", CORROSION, paper no. 572, (Atlanta, GA:NACE International, 2009).

11. R.H. Hausler. "Contribution to the understanding of $H_2S$ corrosion", CORROSION, paper no. 732, (New Orleans, LA:NACE International, 2004).

12. W. Sun and S. Nesic. "A mechanistic model of $H_2S$ corrosion Of mild steel", CORROSION, paper no.655, (Nashville, TN:NACE International, 2007).

13. G. Svenningsen, A. Palencsár, and J. Kvarekvål. "Investigation of iron sulfide surface layer growth in aqueous $H_2S/CO_2$ environments", CORROSION, paper no.359, (Atlanta, GA: NACE International, 2009).

14. H. Ma, X. Cheng, G. Li, S. Chen, Z. Quan, S. Zhao, and L. Niu, "The influence of hydrogen sulfide on corrosion of iron under different conditions", Corrosion Science, 42, 10 (2000): p. 1669-1683.

15. J.-L. Crolet and M.R.Bonis. "Algorithm of the protectiveness of corrosion layers 2-protectiveness mechanisms and $H_2S$ corrosion prediction", CORROSION, paper no. 365, (San Antonio, TX:NACE International: NACE International, 2010).

16. K. Videm and J. Kvarekvål, "Corrosion of carbon steel in carbon dioxide-saturated solutions containing small amounts of hydrogen sulfide", Corrosion, 51, 04 (1995).

17. Y. Zheng, J. Ning, B. Brown, and S. Nesic. "Electrochemical model of mild steel corrosion in a mixed $H_2S/CO_2$ aqueous environment", CORROSION, paper no. 7, (San Antonio, TX : NACE International, 2014).

18. Y. Zheng, B. Brown, and S. Nešić, "Electrochemical study and modelling of $H_2S$ corrosion of mild steel", Corrosion, 70, 4 (2013): p. 351-365.

19. J. Tang, Y. Shao, J. Guo, T. Zhang, G. Meng, and F. Wang, "The effect of $H_2S$ concentration on the corrosion behavior of carbon steel at 90°C", Corrosion Science, 52, 6 (2010): p. 2050-2058.

20. B. Brown and S. Nesic. "Aspects of localized corrosion in an $H_2S$-$CO_2$ environment", CORROSION, paper no. 1559, (Salt Lake City, UT:NACE International, 2012).

21. A.S.T.M. International, *ASTM G46-94 Standard Guide for Examination and Evaluation of Pitting Corrosion*, 2005, ASTM International: West Conshohocken, PA. p. 7.

22. A. Dugstad. "Fundamental Aspects of CO2 Metal Loss Corrosion - Part 1: Mechanism", Corrosion: NACE International, 2006).

23. S. Nesic, J. Postlethwaite, and S. Olsen, "An electrochemical model for prediction of corrosion of mild steel in aqueous carbon dioxide solutions", Corrosion, 52, 04 (1996).

24. J. Kittel, F. Ropital, F. Grosjean, E.M.M. Sutter, and B. Tribollet, "Corrosion mechanisms in aqueous solutions containing dissolved H2S. Part 1: Characterisation of H2S reduction on a 316L rotating disc electrode", Corrosion Science, 66, 0 (2013): p.324-329.

25. C. De Waard and D.E. Milliams, "Carbonic Acid Corrosion of Steel", Corrosion, 31, 5 (1975): p. 177-181.

26. J.L. Crolet, N. Thevenot, and S. Nesic, "Role of Conductive Corrosion Products in the Protectiveness of Corrosion Layers", Corrosion, 54, 3 (1998): p. 194-203.

27. H.Y. Jeong, J.H. Lee, and K.F. Hayes, "Characterization of synthetic nanocrystalline mackinawite: Crystal structure, particle size, and specific surface area", Geochimica et Cosmochimica Acta, 72, 2 (2008): p. 493-505.

28. M. Mullet, S. Boursiquot, M. Abdelmoula, J.-M. Génin, and J.-J. Ehrhardt, "Surface chemistry and structural properties of mackinawite prepared by reaction of sulfide ions with metallic iron", Geochimica et Cosmochimica Acta, 66, 5 (2002): p. 829-836.